Inorganic Chemistry
Article

Photothermally Induced Bergman Cyclization of Metalloenediynes via Near-Infrared Ligand-to-Metal Charge-Transfer Excitation

Brian J. Kraft,[†] Nicole L. Coalter,[†] Mahendra Nath,[†] Aurora E. Clark,[†] Allen R. Siedle,[‡] John C. Huffman,[†] and Jeffrey M. Zaleski*,[†]

Department of Chemistry and Biochemistry, Indiana University, Bloomington, Indiana 47405, and 3M Corporate Research Laboratories, St. Paul, Minnesota 55144

Reaction of 1,2-bis(*tert*-butyldimethylsilyloxy)-4,5-diiodobenzene with 2 equiv of phenylacetylene followed by deprotection with KF/HBr yields the catechol-enediyne ligand 4,5-bis(phenylethynyl)benzene-1,2-diol (CatED, **1**). Metathesis of VO(SALIMH)ACAC·CH$_3$OH (**2**) with **1** and subsequent air oxidation yields (4,5-bis(phenylethynyl)-1,2-dihydroxyphenyl)[4-(2-(salicylideneamino)ethyl)imidazolyl]oxovanadium(V)·CH$_3$OH [VO(SALIMH)CatED], (**3**), in 85%. The thermal Bergman cyclization temperature for **3** is very high (246 °C), which is expected for a rigid, benzannulated enediyne motif. The electronic spectrum of **3** exhibits two strong ligand-to-metal charge transfer (LMCT) transitions centered at 584 nm ($\epsilon = 6063$ M^{-1} cm^{-1}) and 1028 nm ($\epsilon = 8098$ M^{-1} cm^{-1}). These transitions derive from CatED-to-V(V) ligand-to-metal charge transfer, the assignment of which is verified by resonance enhancement of several CatED vibrational modes in the Raman spectra obtained with $\lambda = 785$ vs $\lambda = 457.9$ nm under low power and/or temperature conditions. At elevated temperatures (113–323 K) and powers (2–5 mW), excitation of **3** in the solid state with $\lambda = 785$ nm leads to generation of a black, sparingly soluble, fluorescent product that exhibits weak vibrational features in the 580–600, 1200–1350, and 1450–1600 cm^{-1} regions, indicative of V–O (CatED) and aromatic ring units. The C=C ring modes correspond well with the vibrational characteristics of poly(*p*-phenylene) and derivatives thereof. Additionally, materials generated in both the solid-state thermal and photothermal reactions of **3** demonstrate the formation of high molecular weight species ranging from 5000 to 274 000. On the basis of these data and the literature precedent for formation of poly(*p*-phenylene) via thermolysis of simple enediynes, the reaction poses a unique approach for photoinitiating Bergman cyclization with long-wavelength excitation, as well as the generation of polymeric products.

Introduction

The remarkable reactivity of the enediyne motif has facilitated efforts toward the exploitation of the unusual 1,4-phenyl diradical intermediate for potential therapeutic applications.[1–4] The inability to initiate and control the reactivity of enediynes is, however, one of the primary impediments in the realization of such goals. Transition metals are now known to both stabilize and activate

enediynes toward thermally initiated Bergman cyclization,[5–12] depending on two general factors: the conformational flexibility of the enediyne ligand coordinated to the metal ion[13] and the specific geometry of the chelated metalloenediyne complex.[14–18] Somewhat less clear but equally intriguing is

---

*To whom correspondence should be addressed. E-mail: zaleski@indiana.edu.

† Indiana University.

‡ 3M Corporate Research Laboratories.

(1) Smith, A. L.; Nicolaou, K. C. *J. Med. Chem.* **1996**, *39*, 2103–2117.
(2) Nicolaou, K. C.; Smith, A. L. *The Enediyne Antibiotics*; VCH: Weinheim, Germany, 1995.
(3) Nicolaou, K. C.; Smith, A. L.; Wendeborn, S. V.; Hwang, C. K. *J. Am. Chem. Soc.* **1991**, *113*, 3106–3114.
(4) Nicolaou, K. C.; Smith, A. L.; Yue, E. W. *Proc. Natl. Acad. Sci. U.S.A.* **1993**, *90*, 5881–5888.

(5) Basak, A.; Shain, J. C. *Tetrahedron Lett.* **1998**, *39*, 3029–3030.
(6) Basak, A.; Rudra, K. R. *Tetrahedron Lett.* **2000**, *41*, 7231–7234.
(7) Basak, A.; Shain, J. C.; Khamari, U. K.; Rudra, K. R.; Basak, A. *J. Chem. Soc., Perkin Trans. 1* **2000**, 1955–1964.
(8) König, B.; Hollnagel, H.; Ahrens, B.; Jones, P. G. *Angew. Chem., Int. Ed. Engl.* **1995**, *34*, 2538–2540.
(9) König, B.; Pitsch, W.; Thondorf, I. *J. Org. Chem.* **1996**, *61*, 4258–4261.
(10) König, B. *Eur. J. Org. Chem.* **2000**, 381–385.
(11) O'Connor, J. M.; Lee, L. I.; Gantzel, P.; Rheingold, A. L.; Lam, K.-C. *J. Am. Chem. Soc.* **2000**, *122*, 12057–12058.
(12) Warner, B. P.; Millar, S. P.; Broene, R. D.; Buchwald, S. L. *Science* **1995**, *269*, 814–816.
(13) Rawat, D. S.; Zaleski, J. M. *Chem. Commun.* **2000**, 2493–2494.
(14) Benites, P. B.; Rawat, D. S.; Zaleski, J. M. *J. Am. Chem. Soc.* **2000**, *122*, 7208–7217.

the role that metal ions may play in photochemically initiated enediyne cyclization. For example, electronic excitation ($\lambda \geq 395$ nm) of bis(pyridyl-3-oxy)enediyne complexes of copper results in the formation of Bergman cyclized products, whereas photoexcitation of the free ligand and the Zn^{2+} analogues do not.[19]

Although photoelectronic Bergman cyclization reactions are emerging experimentally and are mechanistically important,[20-22] the ability to employ longer excitation wavelengths would have distinct advantages for biomedical applications such as photodynamic therapy, due to enhanced tissue penetration of near-infrared (near-IR) photons.[23-26] However, photo-Bergman cyclization reactions with long wavelengths ($\lambda > 600$ nm) have not been reported to date, likely due in part to the absence of strongly absorbing electronic transitions in this spectral region for typical enediyne compounds. This notwithstanding, there exist several strategies for the design of molecules with electronic transitions that could potentially lead to photoreactivity with near-IR excitation. The most obvious design involves the preparation of extended organic structures with considerable π-conjugation. In addition to being synthetically challenging, large molecules of this type will likely be insoluble without significant peripheral functionalization. As an alternative, long-wavelength electronic transitions with considerable absorptivity can be generated via metal−ligand charge transfer within compounds where both metal oxidation state and donor/acceptor ligand redox potential have been judiciously chosen.[27] Unfortunately, the mechanistic description of the photo-Bergman reaction[20-22] is not well-established for a wide variety of chemical architectures and therefore does not mandate (or preclude) that metal−ligand charge-transfer excitation necessarily leads to photo-Bergman reactivity. The realization of strongly absorbing, near-IR transitions of this type does, however, suggest the potential for designing metalloenediyne constructs that can lead to photoinduced Bergman cyclization through a photothermal route involving nonradiative excited-state decay, rather than the established electronic excitation pathways.[20,22]

To test this concept, we have prepared a novel V(V) metalloenediyne compound of the new 4,5-bis(phenylethynyl)benzene-1,2-diol (CatED, 1) ligand. The V(V) metalloenediyne exhibits strong ligand-to-metal charge-transfer (LMCT) transitions in the near-IR spectral region due to the low redox potentials of the high-valent vanadium center and the easily oxidized catechol metal binding motif. A combination of differential scanning calorimetry (DSC) and resonance Raman data show that these LMCT transitions can be used to photothermally activate the V(V) metalloenediyne compound toward Bergman cyclization upon 785 or 1064 nm laser excitation, despite the compound's relative inertness to photo-Bergman reactivity upon electronic excitation in the ultraviolet spectral region.

Experimental Section

Materials. 1,2-Diiodoveratrole, 4,5-diiodobenzene-1,2-diol, 1,2-bis(*tert*-butyldimethylsilyloxy)-4,5-diiodobenzene, 4-(2-(salicylideneamino)ethyl)imidazole, and (acetylacetonato)[4-(2-(salicylideneamino)ethyl)imidazolyl]oxovanadium(IV)·CH$_3$OH [VO-(SALIMH)ACAC·CH$_3$OH, **2**] were prepared according to literature procedures.[28-31] VO(ACAC)$_2$ was purchased from Strem, while all other materials were purchased from Aldrich and used as received. Solvents were dried (distillation or sieves) and degassed according to standard procedures prior to use.

Physical Measurements. A nitrogen-atmosphere drybox was used for all air-sensitive manipulations. ^{1}H (400 MHz) and ^{13}C{^{1}H} (101 MHz) NMR spectra were obtained on a Varian Unity I400 spectrometer and were referenced to the residual proton signal of the solvent. Differential scanning calorimetry traces were recorded on a V4.1 Dupont 910 DSC differential scanning calorimeter coupled to DuPont thermal analyst 2100 at a heating rate of 10 °C min^{-1}. Infrared spectra were recorded as KBr pellets on a Nicolet 510P spectrophotometer. Cyclic and differential pulse voltammograms were recorded on a BAS CV 50 W voltammetric analyzer utilizing a glassy carbon working electrode, a platinum auxiliary electrode, and an SCE reference electrode. Potentials are quoted versus SCE. Electronic absorption spectra were recorded on a Perkin-Elmer Lamba 19 using UVWinlab software. Raman spectra were collected with a Renishaw 1000B micro-Raman spectrometer operating with a 785 nm SDL diode laser or a Coherent I-70 Ar$^+$ ion laser (457.9 nm) under variable power (0.2−20 mW) conditions. Temperature-dependent Raman spectra were obtained using a Linkam model TDS 600 variable temperature hot-state/cold-stage assembly that was mounted directly on the Raman microscope stage. Crystallographic data were collected on a Bruker-AXS SMART6000 CCD system using a sealed Cu source and graphite monochromator. The sample was cooled using a nitrogen gas-flow cooling system of local design.

Synthesis of 1,2-Bis(*tert*-butyldimethylsilyloxy)-4,5-bis(phenylethynyl)benzene. Dichlorobis(triphenylphosphine)palladium(II) (351

(15) Chandra, T.; Pink, M.; Zaleski, J. M. *Inorg. Chem.* **2001**, *40*, 5878−5885.
(16) Rawat, D. S.; Benites, P. J.; Incarvito, C. D.; Rheingold, A. L.; Zaleski, J. M. *Inorg. Chem.* **2001**, *40*, 1846−1857.
(17) Coalter, N. L.; Concolino, T. E.; Streib, W. E.; Hughes, C. G.; Rheingold, A. L.; Zaleski, J. M. *J. Am. Chem. Soc.* **2000**, *122*, 3112−3117.
(18) Schmitt, E. W.; Huffman, J. C.; Zaleski, J. M. *Chem. Commun.* **2001**, 167−168.
(19) Benites, P. B.; Holmberg, R.; Rawat, D. S.; Kraft, B. J.; Klein, L. J.; Peters, D. G.; Thorp, H. H.; Zaleski, J. M. *J. Am. Chem. Soc.*, submitted for publication.
(20) Evenzahav, A.; Turro, N. J. *J. Am. Chem. Soc.* **1998**, *120*, 1835−1841.
(21) Kaneko, T.; Takahashi, M.; Hirama, M. *Angew. Chem., Int. Ed.* **1999**, *38*, 1267−1268.
(22) Clark, A. E.; Davidson, E. R.; Zaleski, J. M. *J. Am. Chem. Soc.* **2001**, *123*, 2650−2657.
(23) Mody, T. M.; Sessler, J. L. In *Supramolecular Materials and Technologies*; Reinhoudt, D. N., Ed.; Wiley: Chichester, U.K., 1999; Vol. 4, p 245.
(24) Ali, H.; van Lier, J. E. *Chem. Rev.* **1999**, *99*, 2379−2450.
(25) Boyle, R. W.; Dolphin, D. *Photochem. Photobiol.* **1996**, *64*, 469−485.
(26) Dougherty, T. J.; Henderson, B. W.; Schwartz, S.; Winkelman, J. W.; Lipson, R. L. In *Photodynamic Therapy, Basic Principles and Clinical Applications*; Henderson, B. W., Dougherty, T. J., Eds.; Dekker: New York, 1992; p 1.
(27) Lever, A. B. P.; Dodsworth, E. S. In *Electrochemistry, Charge Transfer Spectroscopy, and Electronic Structure*; Solomon, E. I., Lever, A. B. P., Eds.; Wiley: New York, 1999; Vol. 2, p 227.
(28) Suzuki, H.; Nakamura, K.; Goto, R. *Bull. Chem. Soc. Jpn.* **1966**, *39*, 128−131.
(29) Cornman, C. R.; Kampf, J.; Peocoraro, V. L. *Inorg. Chem.* **1992**, *31*, 1981−1983.
(30) Cornman, C. R.; Colpas, G. J.; Hoeschele, J. D.; Kampf, J.; Pecorraro, V. L. *J. Am. Chem. Soc.* **1992**, *114*, 9925−9933.
(31) Kinder, J. D.; Youngs, W. J. *Organometallics* **1996**, *15*, 460−463.

mg, 0.5 mmol) and copper iodide (190 mg, 1 mmol) were charged to a flask, and 100 mL each of benzene and diisopropylamine were added. To this solution, 1,2-bis(*tert*-butyldimethylsilyloxy)-4,5-diiodobenzene (6.0 g, 0.01 mol) was introduced. In 10 mL of benzene, phenylacetylene (2.5 mL, 0.023 mol) was added dropwise and the reaction was stirred for 3 h. The catalysts were removed by filtration through a silica gel bed, and the filtrate was concentrated and purified by flash chromatography (10% ethyl acetate/hexanes). Yield: 75%. ^{1}H NMR (CDCl$_3$; ppm): δ 7.55 (m, 4H), 7.35 (m, 6H), 7.04 (s, 2H), 1.01 (s, 18H), 0.26 (s, 12H). ^{13}C NMR (CDCl$_3$; ppm): δ 148.1, 131.8, 128.8, 128.6, 124.4, 123.8, 119.6, 92.2, 88.5, 26.0, 18.7, -3.9. EI MS: [M$^+$] 538.3.

Synthesis of 4,5-Bis(phenylethynyl)benzene-1,2-diol (CatED, 1). A flask was charged with 4 equiv of KF. Anhydrous dimethylformamide (DMF; 18 mL) and 0.1 equiv of 48% HBr were added, and the flask was cooled to 0 °C. 1,2-Bis(*tert*-butyldimethylsilyloxy)-4,5-bis(phenylethynyl)benzene (1 equiv) was dissolved in 5 mL of anhydrous DMF and added dropwise to the KF/HBr solution. After 24 h of stirring, 100 mL of cooled 2 M HCl was added and the product subsequently extracted with ether (3 × 50 mL), washed with brine, dried with MgSO$_4$, and concentrated. Yield: 80%. ^{1}H NMR (CD$_2$Cl$_2$; ppm): δ 7.55 (m, 4H), 7.35 (m, 6H), 7.04 (s, 2H). ^{13}C NMR (CD$_2$Cl$_2$; ppm): δ 155.9, 130.2, 124.6, 119.9, 118.6, 117.4, 116.6, 97.4, 87.5.

Synthesis of (4,5-Bis(phenylethynyl)-1,2-dihydroxyphenyl)-[4-(2-(salicylideneamino)ethyl)imidazolyl]oxovanadium(V)· CH$_3$OH (VO(SALIM)CatED, 3). Compound 2^{29,30} (508 mg, 1.2 mmol) was dissolved in 50 mL of dry acetonitrile. To this solution was added 1 (470 mg, 1.3 mmol). Although the color of the solution turned immediately from red to deep blue, it was allowed to stir for 12 h in air. A dark blue precipitate formed and was filtered and dried. The filtrate was added to a round-bottom flask and subsequently dried under vacuum. The residue was dissolved in a minimal amount of CH$_2$Cl$_2$, and twice the volume of hexanes was added to precipitate the remaining product. X-ray quality crystals were grown by slow diffusion of hexanes into chloroform. Yield: 85%. ^{1}H NMR (CD$_2$Cl$_2$; ppm): δ 10.45 (bs, 1H); 8.39 (s, 1H); 7.58 (s, 1H); 7.49 (m, 5H); 7.38 (m, 7H); 6.84 (m, 4H); 6.36 (s, 1H); 4.07 (s, 2H); 3.04 (m, 2H). Anal. Calcd for (VC$_{34}$H$_{24}$N$_3$O$_4$· CH$_3$OH): C, 67.7; H, 4.5; N, 7.2. Found: C, 67.9; H, 3.99; N, 7.12.

Crystallographic Structure Determination for 3. Crystals consisted of thin black needles growing on the side of the sample flask and were typically less than 40 μm thick, with widths of several tenths of a millimeter and lengths up to 0.7 mm. A crystal of 30 × 100 × 300 μm was examined and appeared to be essentially untwinned, although diffraction was weak. The crystal was affixed to the side of a glass fiber using silicone grease and cooled to 112 K for data collection. The data were collected using 60 s frames with an ω scan of 0.30°. Data were corrected for Lorentz and polarization effects, and equivalent reflections were averaged using the Bruker SAINT software as well as utility programs from the XTEL library. An absorption correction was performed using the SADABS program supplied by Bruker AXS. The structure was solved using SHELXTL and Fourier techniques. Statistical tests indicated that the correct space group was the noncentrosymmetric *Pca*2$_1$ with $Z = 8$. The fact that the two independent molecules appeared to be related by a center of inversion led to a careful examination of the centrosymmetric space group (*Pcam*) as an alternate choice. Attempts to refine in *Pcam* were unsuccessful. Examination of the final parameters indicates that there are small but significant differences in the two molecules. These are readily apparent in the best molecular fit (BMFIT) analysis. Because of

the small size of the crystal and the weak intensities, only the metal atoms were refined anisotropically. Hydrogen atoms were placed in fixed idealized positions. A final difference Fourier was essentially featureless with maximum peak heights of 0.53 e/A^3. Since there are two independent molecules, all chemically equivalent distances and angles are identical in the two, within experimental error.

Thermolysis of 1. To a degassed solution of **1** (0.04 g, 0.13 mmol) in 30 mL of chlorobenzene, 3.0 mL (39.2 mmol) of dry, degassed 2-propanol was added. The resulting mixture was maintained at 180 °C sealed in a high-pressure reaction tube submerged in silicone oil for 90 h. After cooling to room temperature, the reaction mixture was loaded onto a silica gel column and the chlorobenzene was removed by eluting with hexane. The crude product mixture was removed from the column via elution with ethyl acetate. The cyclized product was subsequently purified on preparative thin-layer chromatography (TLC) (ethyl acetate:hexane, 30:70). Yield 45%. ^{1}H NMR (CD$_3$OD; ppm): δ 7.44−7.30 (m, 10H); 6.90 (s, 1H); 6.72 (s, 1H); 6.60 (s, 1H); 4.30 (sept, 1H); 1.10 (d, 6H).^{13}C NMR (CD$_3$OD; ppm): δ 144.5, 141.2, 139.1, 136.4, 134.1, 132.1, 130.3, 129.5, 129.1, 128.5, 128.4, 127.8, 126.5, 112.4, 106.4, 74.1, 22.8. HR-MS (EI) *m/z*. Calcd for C$_{25}$H$_{22}$O$_3$ (M$^+$): 370.1568. Found: 370.1561.
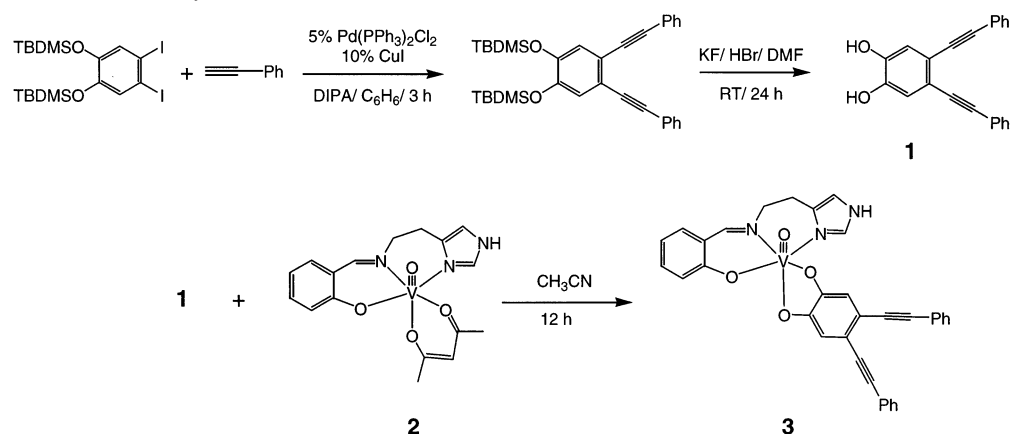
Polymer Characterization. For size exclusion chromatography (SEC), ∼100 μL of a given solution was injected into a Polymer Labs PLGEL mixed C column (heated to 46 °C) using a Shimadzu LC-2010A chromatograph. The system operated at room temperature using DMF containing ∼0.01 M LiBr as the eluent and flow rates of ∼1−0.5 mL/min. Changes in concentration were detected by a Shimadzu RID 10A refractive index detector. The molecular weight calculations (Caliber Software, Polymer Labs) were based upon a calibration made of narrow dispersity polystyrenes ranging in molecular weight from 580 to 7.5 × 10^6 amu.

Thermal Solution Polymerization of 1. A solution of 0.050 g (0.16 mmol) of **1** in 5 mL of chlorobenzene was maintained at 180 °C in a high-pressure reaction tube submerged in silicone oil for 48 h. Over the course of the reaction, the solution turned from a pale yellow to a dark brown/black. After completion, the solvent was removed under vacuum on a Schlenk line. The black, gummy residue was then dissolved in ∼1 mL of DMF and subjected to SEC analysis.

Thermal Solution Polymerization of 3. A solution of 0.050 g (0.085 mmol) of **3** in 5 mL of benzonitrile was maintained at 270 °C for 48 h in a high-pressure reaction tube submerged in sand. Over the course of the reaction, the solution turned from a dark blue to a dark brown/black color. After completion, the solvent was removed under vacuum. To the resulting black oil, ∼3 mL of DMF was added, and the resulting solution was subjected to SEC analysis.

Solid-State Thermal Polymerization of 3. A 30 mg sample of **3** was uniformly spread onto a glass slide which was placed in a Linkam model TDS 600 variable temperature hot stage. The sample was subsequently heated to a temperature of 240 °C for a period of 24 h. Over the course of heating, the sample decreased in volume, forming brown/black clumps. The sample was then suspended in 10 mL of DMF containing 0.01 M LiBr. After being shaken for several hours, the solution was filtered using a 0.2 μm Nylon Titan syringe filter. The filtrate was then subjected to SEC anlysis.

Photothermal Polymerization of 3. For bulk photothermal polymerization, a 30 mg sample of **3** was spread uniformly onto a glass slide over a 1 × 0.5 in. area. A 785 nm SDL diode laser operating at 100 mW was then gently focused through a 5× objective to maximize sample coverage, and traversed across the

Scheme 1. Synthesis of Metalloenediyne **3**

Table 1. Crystallographic Data for **3**

formula	$C_{34}H_{24}N_3O_4V$
fw	589.52
color of cryst	Black
cryst syst	orthorhombic
space group	$Pca2_1$
a, Å	21.0202(26)
b, Å	6.5554(7)
c, Å	42.175(4)
α, deg	90
β, deg	90
γ, deg	90
V, Å^3	5811.5
Z	8
ρ_{calcd}, g/cm^3	1.348
T, K	112
λ, Å	0.710 73
$R(F_o)^a$	0.060
$R_w(F_o)^b$	0.043

^{a} $R = \sum |F_o| - |F_c|/\sum |F_o|$. ^{b} $R_w = [\sum w(|F_o| - |F_c|)^2/\sum w|F_o|^2]^{1/2}$, where $w = 1/\sigma^2(|F_o|)$.

sample area in a grid pattern over the course of 3 h (15 min/pass, 10 passes) after which the blue sample was converted to a gray/black powder. The sample was then transferred to a 1 mL sample vial, and 500 μL of DMF was added. After addition of DMF the sample was sonicated and subjected to mild heat until the bulk of the material had dissolved (1−2 min). The resulting solution was then subjected to SEC analysis.

Computational Methods and Vibrational Analysis. Geometry optimization of **3** was performed using density functional theory (DFT) and the B3LYP combination of functionals available in Gaussian 98.[32] The LANL effective core potential and the LANL2DZ basis was used for V and O, while the 6-31G basis set was used for the C, N, and H. Since the crystal structure of **3** was not an energetic minimum in the gas phase, only the vibrational analysis at the gas-phase B3LYP optimized geometry of **3** is presented here. The DFT vibrational frequencies were scaled by 0.9613, which is customary for the B3LYP method and the 6-31G(d) basis set for organic molecules.[33] Use of this scaling factor resulted in values that were in good agreement with the experimental results for known vibrations such as C≡C.

Results and Discussion

Syntheses of 1−3. 4,5-Bis(phenylethynyl)benzene-1,2-diol (**1**) was prepared by coupling phenylacetylene to the protected 1,2-bis(*tert*-butyldimethylsilyloxy)-4,5-diiodo-benzene via in situ formation of the copper acetylide precursor to yield 1,2-bis(*tert*-butyldimethylsilyloxy)-4,5-bis(phenylethynyl)benzene. Subsequent fluoride-promoted deprotection of the *tert*-butyldimethylsilyloxy functionality gives the diol **1** in 80% yield (Scheme 1). Addition of **1** to a room-temperature solution of **2**[29] in dry CH$_3$CN produces the product **3** in 85% yield. The X-ray structure of **3** (vide

(32) Frisch, M. J.; Trucks, G. W.; Schlegel, H. B.; Scuseria, G. E.; Robb, M. A.; Cheeseman, J. R.; Zakrzewski, V. G.; Montgomery, J. A. J.; Stratmann, R. E.; Burant, J. C.; Dapprich, S.; Millam, J. M.; Daniels, A. D.; Kudin, K. N.; Strain, M. C.; Farkas, O.; Tomasi, J.; Barone, V.; Cossi, M.; Cammi, R.; Mennucci, B.; Pomelli, C.; Adamo, C.; Clifford, S.; Ochterski, J.; Petersson, G. A.; Ayala, P. Y.; Cui, Q.; Morokuma, K.; Malick, D. K.; Rabuck, A. D.; Raghavachari, K.; Foresman, J. B.; Cioslowski, J.; Ortiz, J. V.; Baboul, A. G.; Stefanov, B. B.; Liu, G.; Laishenko, A.; Piskorz, P.; Komaromi, I.; Gomperts, R.; Martin, R. L.; Fox, D. J.; Keith, T.; Al-Laham, M. A.; Peng, C. Y.; Nanayakkara, A.; Gonzalez, C.; Callacombe, M.; Gill, P. M. W.; Head-Gordon, M.; Replogle, E. S.; Pople, J. A. *Gaussian 98*, A.6 ed.; Gaussian, Inc.: Pittsburgh, PA, 1998.

(33) Foresman, J. B.; Frisch, E. *Exploring Chemistry with Electronic Structure Methods*, 2nd ed.; Gaussian Inc.: Pittsburgh, PA, 1996.
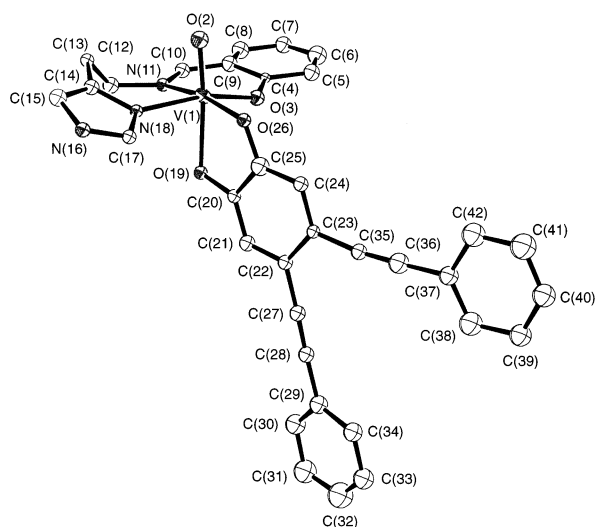
infra), NMR (^{1}H, ^{13}C), mass spectrometry, and elemental analysis confirm the identity of the product.

X-ray Crystal Structure of 3. Crystals of **3** for X-ray structure determination were obtained by layering and slow diffusion of hexanes into chloroform. The structure of **3** (Table 1) exhibits a six coordinate, disordered octahedral VO^{3+} center with N$_2$O$_3$ ligation from the imidazole, imine, and phenoxy functionalities of the SALIMH ligand as well as the chelating catechol-enediyne ligand **1** (Figure 1). The immediate structure about the V(V) ion is very similar to the catecholate analogue previously reported[30] with only minor deviations in bond distances and angles (Table 2). The V−O(2) bond is short (1.64 Å), indicating that the multiple bond character of the V≡O unit remains intact. As a consequence of the strong orbital overlap along the *z*-axis, the V−O(19) bond trans to the oxo ligand is elongated (2.18 Å), while the V−O(3) and V−O(26) bonds in the *xy*-plane are considerably shorter with distances of 1.90 and 1.91 Å, respectively. The V−N bond distances to the imine nitrogens (V−N(11) and V−N(18)) are nearly identical at 2.1 Å. The distorted octahedral geometry is further reflected in the deviation from linearity of the O(2)−V(1)−O(19) and the O(3)−V(1)−N(18) angles which are 166 and 164°, respectively. Finally, the through-space alkyne termini separation (C(28)−C(36)) is 4.3 Å which is large, implying a thermally

Figure 1. ORTEP of the X-ray crystal structure of **3**. Thermal ellipsoids are illustrated at 50% probability.

Table 2. Selected Bond Distances (Å) and Bond Angles (deg) for **3**

bond/angle	exptl	calcd
V(1)−O(2)	1.643(10)	1.606
V(1)−O(3)	1.901(9)	1.868
V(1)−O(19)	2.180(9)	2.152
V(1)−O(26)	1.913(10)	1.841
V(1)−N(11)	2.124(12)	2.110
V(1)−N(18)	2.102(11)	2.158
O(2)−V(1)−O(3)	106.1(5)	98.3
O(2)−V(1)−O(19)	166.4(4)	170.9
O(2)−V(1)−O(26)	96.6(4)	101.0
O(2)−V(1)−N(11)	95.7(5)	98.4
O(2)−V(1)−N(18)	88.8(5)	89.1
O(3)−V(1)−O(19)	85.8(4)	90.8
O(3)−V(1)−O(26)	88.5(4)	99.6
O(3)−V(1)−N(11)	86.8(4)	84.0
O(3)−V(1)−N(18)	164.1(4)	167.7
O(19)−V(1)−O(26)	76.6(4)	78.2
O(19)−V(1)−N(11)	91.6(4)	81.6
O(19)−V(1)−N(18)	80.2(4)	81.8
O(26)−V(1)−N(11)	167.6(4)	159.5
O(26)−V(1)−N(18)	95.4(4)	88.5
N(11)−V(1)−N(18)	86.3(4)	85.3

stable framework based on correlations with other rigid enediyne linkages.[1,16,34−37]

Electronic Structure and Vibrational Analyses. Compound **3** exhibits two low-energy CatED oxygen-to-V(V) LMCT transitions at 584 nm ($\epsilon = 6063$ M^{-1} cm^{-1}) and 1028 nm ($\epsilon = 8098$ M^{-1} cm^{-1}) (Figure 2). The low-energy transition is significantly red shifted relative to other V(V)−catechol complexes[30,38] due to electronic delocalization into the enediyne framework. Electrochemical studies show that the catechol-enediyne ligand is irreversibly oxidized at 1.0 V vs SCE and the vanadium(V/IV) redox couple is very modest ($E_{1/2} = -200$ mV vs SCE). Using the ΔE(redox) approximation for the LMCT energy between the HOMO

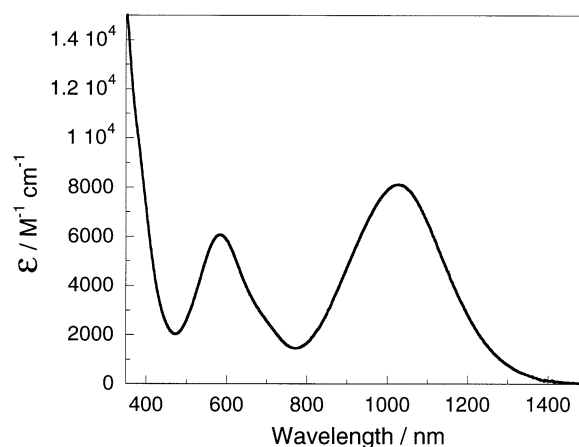**Figure 2.** Electronic absorption spectrum of **3** in CH$_2$Cl$_2$ recorded at 298 K.

and LUMO,[27,39] $\Delta E = 1.2$ V or ∼1032 nm, which correlates very well with the observed low-energy optical transition. The higher energy band is also associated with CatED-to-V(V) LMCT since two sets of charge-transfer transitions are expected from out-of-plane, metal−oxygen π-bonding interactions.[30,38,40,41] However, the higher energy absorption is complicated by phenoxy-to-V(V) transitions from the ancillary SALIMH ligand which occur in the same spectral region.[38] The interpretation is consistent with previous reports of the electronic structure of oxovanadium(V) compounds with analogous ligand sets (e.g. VO(SALIMH)(cat.): $\lambda_1 = 540$ nm, $\epsilon = 4000$ M^{-1} cm^{-1}; $\lambda_2 = 920$ nm, $\epsilon = 4500$ M^{-1} cm^{-1}),[30] as well as [V(cat.)$_3$]$^-$ ($\lambda_1 = 625$ nm, $\epsilon = 13\,000$ M^{-1} cm^{-1}; $\lambda_2 = 900$ nm, $\epsilon = 17\,000$ M^{-1} cm^{-1}).[38] These studies document that the donor orbitals for both LMCT transitions have dominant contributions from the bidentate CatED chelate.

The IR and Raman spectra of VO(SALIMH)(CatED) are presented in Figure 3 and Table 3. The assignments of the vibrations in these spectra derive from both the DFT vibrational analysis of **3** at the optimized gas-phase geometry (Table 2), as well as the IR and/or Raman data for **1**, catechol, and VO(SALIMH)(ACAC).[42] Since the crystal structure of **3** was not an energetic minimum in the gas phase, only the vibrational analysis at the gas-phase B3LYP optimized geometry of **3** is presented here. Relevant structural differences between the crystal structure and the B3LYP geometry are shown in Table 2.

The IR spectrum of **3** (Figure 3a) exhibits considerable intensity in vibrational modes generally associated with the phenoxy and catechol rings of the SALIMH and CatED ligands, respectively. These vibrations in the free ligands are shifted by only ∼ 10 cm^{-1} or less upon complexation to vanadium and occur within the customary range for substituted aromatic rings (1400−1600 and 700−900 cm^{-1}). The

(34) Schreiner, P. R. *J. Am. Chem. Soc.* **1998**, *120*, 4184−4190.
(35) Koseki, S.; Fujimura, Y.; Hirama, M. *J. Phys. Chem. A* **1999**, *103*, 7672−7675.
(36) Jones, G. B.; Warner, P. M. *J. Am. Chem. Soc.* **2001**, *123*, 2134−2145.
(37) Kim, C.; Russell, K. C. *J. Org. Chem.* **1998**, *63*, 8229−8234.
(38) Cooper, S. R.; Koh, Y. B.; Raymond, K. N. *J. Am. Chem. Soc.* **1982**, *104*, 5092−5102.
(39) Vlcek, A. A. *Electrochim. Acta* **1968**, *13*, 1063−1078.
(40) Cox, D. D.; Benkovic, S. J.; Bloom, L. M.; Bradley, F. C.; Nelson, M. J.; Que, L.; Wallick, D. E. *J. Am. Chem. Soc.* **1988**, *110*, 2026−2032.
(41) Karpishin, T. B.; Gebhard, M. S.; Solomon, E. I.; Raymond, K. N. *J. Am. Chem. Soc.* **1991**, *113*, 2977−2984.
(42) Data included in Supporting Information.

Table 3. Experimental and Theoretical Vibrational Frequencies for **3**

vibrational mode[a]	B3LYP/6-31G// LANL2DZ[b] (cm^{-1})	B3LYP/6-31G// LANL2DZ[c] (cm^{-1})	Raman (cm^{-1})	IR (cm^{-1})
ν_{167} C≡C sym stretch	2313	2224	2202	2202
ν_{166} SALIMH C=N; imidazole C=C stretch	1669	1605		1621
ν_{159} CatED C=C ring stretch	1621	1559	1553	1552
ν_{155} CatED C=C ring stretch	1545	1485	1483	
ν_{150} CatED C=C ring stretch	1503	1445	1450	1449
ν_{141} SALIMH phenoxy CO and ring stretch	1397	1342	1338	1339
ν_{136} CatED CO and ring stretch	1351	1299	1304	1308
ν_{126} CatED in-plane CH bend	1272	1223	1213	
ν_{116} SALIMH phenoxy in-plane CH bend	1171	1125	1122	1127
ν_{105} V≡O stretch	994	955		955
ν_{77} CatED C=C ring bend	800	769		757
ν_{72} C(37) and C(29) phenyl out-of-plane CH bend + C=C ring bend	725	697	696	691
ν_{61} C(37) and C(29) phenyl out-of-plane CH bend	655	629		622
ν_{56} CatED VO symmetric stretch	592	569	556	
ν_{48} CatED VO asymmetric stretch	509	489	483	
ν_{37} CatED + SALIMH CC out-of-plane bend (delocalized)	403	387	374	
ν_{34} SALIMH and CatED rocking modes	355	341	338	

[a] Assignments represent the region of the molecule with the greatest atomic displacement. [b] Unscaled values. [c] Scaled by 0.9613.
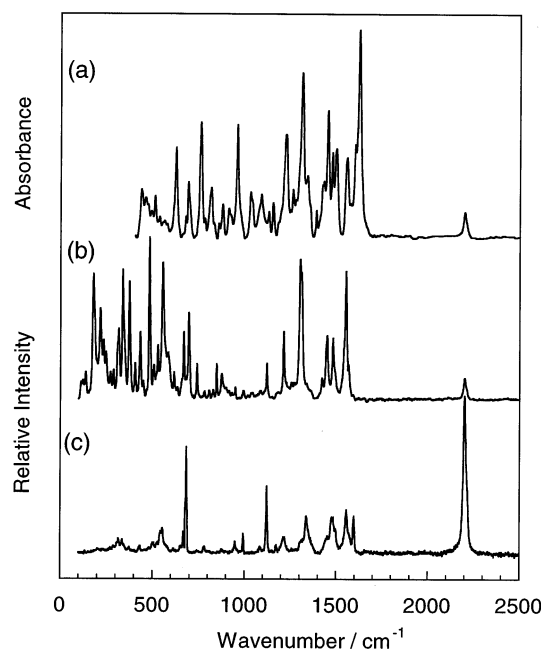

Figure 3. Vibrational spectra of **3**: (a) infrared absorption spectrum (KBr) obtained at ambient temperature; (b) Raman spectrum of **3** in the solid state collected at 80 K with λ = 785 nm; (c) solid-state Raman spectrum of **3** at 85 K using 457.9 nm excitation.

Raman spectrum obtained with λ = 785 nm (Figure 3b) reveals strong resonance enhancement of the metal−CatED vibrations due to the LMCT character of the optical transition centered at 1028 nm (Figure 2). In contrast, the dominant feature of the Raman spectrum obtained with λ = 457.9 nm (Figure 3c) is the alkyne stretch, which has an intensity greater than all other vibrations by a factor of ~1.4. This spectral profile is very similar to those obtained under off-resonance conditions for other enediyne ligands and metallo-enediyne compounds.[18] Additionally, the ν_{116} (1122 cm^{-1}; SALIMH phenoxy in-plane C−H bend) is of low intensity in all spectra, while CatED catechol ring stretches ν_{159} (1553 cm^{-1}), ν_{155} (1483 cm^{-1}), and ν_{150} (1450 cm^{-1}), as well as vibrations ν_{136} (1304 cm^{-1}; CatED C−O stretch) and ν_{126} (1213 cm^{-1}; CatED in-plane C−H bend), which exhibit

substantial enhancement in the λ = 785 nm Raman spectrum relative to that obtained with λ = 457.9 nm. The moderately intense vibration at 955 cm^{-1} (IR) is attributed to the V≡O stretching frequency of the monooxovanadium(V) center and occurs within the expected frequency region of 950−990 cm^{-1}.[43−46] Consistent with previous observations,[44,47] the phenoxy C−O stretch in SALIMH type ligands occurs at ~1320 cm^{-1} and shifts to higher frequency upon complexation to vanadium. Thus, the 1338 (Raman) and 1339 cm^{-1} (IR) bands are assigned to the SALIMH C−O stretch. Similarly, the CatED C−O stretch,[48] which occurs at 1283 cm^{-1} in the free CatED ligand, shifts to higher frequency upon complexation. Lastly, V−O and V−N stretches have been observed for many ligands between 355 and 500 cm^{-1}.[49] The enhancement of the 483 and 556 cm^{-1} bands in the Raman spectrum obtained with λ = 785 nm excitation, as well as the DFT vibrational analysis, lead to the assignment of these vibrations as symmetric and asymmetric V−O stretches involving the CatED ligand.

Thermal Reactivities of 1 and 3 in the Solid State. The thermal reactivity of **1** reveals an exothermic peak in the DSC trace at 165 °C (Figure 4), which is in the range of, but somewhat lower than expected for, a rigid, acyclic, and benzannulated enediyne structure reacting as a neat oil.[13,16] The decreased cyclization temperature of **1** is attributable to the electron donating diol substituents.[13,16,36] DSC traces for ligands such as **1** are frequently broad arising from an ensemble of configurations in the liquid state and often exhibit sloping baselines at postcyclization temperatures due to further reactivity of Bergman cyclized products.[16] Complexation of **1** to generate **3** causes an increase in the

(43) Chakravarty, J.; Dutta, S.; Dey, A.; Chakravorty, A. *J. Chem. Soc., Dalton Trans.* **1994**, 557−561.
(44) Lui, S.-X.; Gao, S. *Polyhedron* **1998**, *17*, 81−84.
(45) Fisher, D. C.; Barclay-Peet, S. J.; Balfe, C. A.; Raymond, K. N. *Inorg. Chem.* **1989**, *28*, 4399−4406.
(46) Pecoraro, V. L. *Inorg. Chim. Acta* **1989**, *155*, 171−173.
(47) Nakamota, K. *Infared and Raman Spectra of Inorganic Coordination Compounds*, 4th ed.; Wiley: New York, 1986.
(48) Gerhards, M.; Perl, W.; Schumm, S.; Henrichs, U.; Jacoby, C.; Kleinermanns, K. *J. Chem. Phys.* **1996**, *104*, 9362−9375.
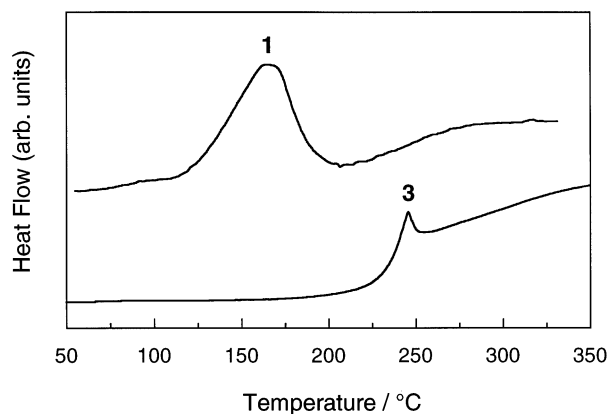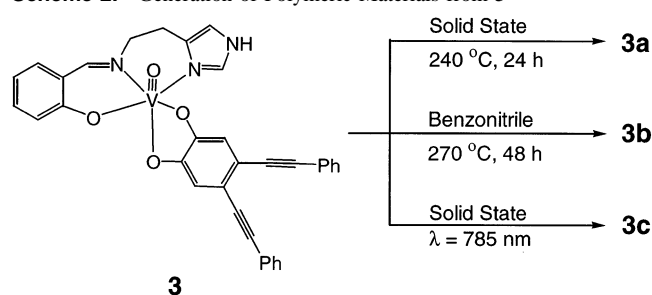(49) Gao, S.; Weng, Z.-Q.; Liu, S.-X. *Polyhedron* **1998**, *17*, 3595−3606.

Figure 4. DSC traces for the thermal reactivities of **1** and **3**. Bergman cyclization of compounds **1** (liquid, 165 °C) and **3** (solid, 246 °C) are indicated by the sharp exothermic features in the profile.

**Scheme 2.** Generation of Polymeric Materials from **3**

observed thermal cyclization temperature of the enediyne functionality to 246 °C (Figure 4). The thermal reactivity of the metal-bound enediyne is in contrast to that observed for enediyne ligands that coordinate metals at functional groups adjacent to the alkyne termini. In those cases, the ligands typically exhibit a decrease in the thermal stability toward Bergman cyclization relative to that of the free ligand due to the ability of the metal center to draw the alkyne termini into close proximity upon coordination.[5-8,12,14,16,17] For **3** this is not the case, and as such, a decrease in the cyclization temperature is not expected. The increased Bergman cyclization temperature of **3** can be primarily attributed to the different physical states of **1** and **3** at their respective cyclization temperatures (oil vs solid). However, electronic contributions to the cyclization temperature cannot be completely ruled out in this case. Relative to diprotonated **1**, the long V−O(19) bond of the catechol-enediyne trans to the oxo ligand may permit a small electronic contribution to the cyclization temperature of **3** arising from an allyl-quinoid resonance form, which should stabilize the formal enediyne motif with respect to Bergman cyclization. The Raman/IR and DFT vibrational analyses also show an increase in the CatED C−O stretch by ~20 cm^{-1}[48] upon complexation of the free ligand (1283 cm^{-1}), indicating donation of lone pair electron density to the metal and partial contribution from the quinoid resonance form in the electronic structure of the complex. Moreover, vibrational spectra for **1** and **3** also show a 10 cm^{-1} decrease of the alkyne stretch upon complexation to the V(V) center (2206 to 2196 cm^{-1}), further suggesting a modest structural contribution from such a resonance form. In light of the phase difference

Table 4. Weight (M_w) and Number Average Molecular Weights (M_n) for Materials **1b** and **3a−c**[a]

compd	M_w	M_n	P^b
1b	10 763	10 245	1.05
3a	81 200	24 500	3.34
3b	5 049, 17 160^c	d	d
3c	5 603	4 170	1.34

[a] Values of M_w and M_n were calculated using polystyrene standards of narrow polydispersity. [b] Polydispersity (P) = M_w/M_n. [c] Peak shoulder extends to 274 000. [d] Due to overlapping peaks in the chromatogram accurate values of M_n and P could not be determined.

Scheme 3. Thermal Reactivity of **1** in Solution
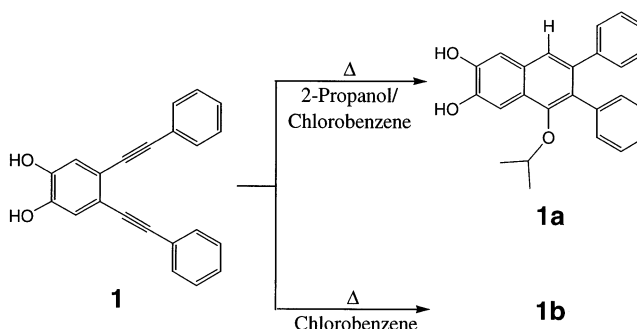
between **1** (oil) and **3** (solid) at the Bergman cyclization temperature, the degree to which this contribution is significant (>20 °C) to the observed reaction temperatures is unclear. However, in light of the increase in the thermal barrier to Bergman cyclization upon introduction of electron withdrawing substituents in the vicinity of the -ene- unit,[36] the electronic structure contribution cannot be dismissed outright.

Characterization of the thermal reaction product obtained from **3** indeed indicates the formation of extended polymeric materials **3a** (Scheme 2, Table 4). Qualitatively, the thermal polymerization of **3** can be observed as a decrease in the volume of the material, while quantitatively, polymeric material with molecular weights (M_w) of 81 200 are observed. It is worth noting that the molecular weight analysis encompasses only the soluble portion of the material, which likely represents only polymer fragments of lower molecular weight. The large body of evidence for the intermediacy of the 1,4-phenyl diradical in the thermal reactivities of both simple organic enediynes[50] and more elaborate metalloenediynes[9,14,51] implicates a polymer product deriving from the Bergman cyclization of **3**.

Thermal Reactivities of 1 and 3 in Solution. In the presence of 2-propanol in chlorobenzene, **1** thermally reacts at 180 °C to yield Bergman cyclized product **1a** (Scheme 3). Interestingly, the 1,4-phenyl diradical appears to insert into the O−H bond of 2-propanol rather than performing H-atom abstraction from either of the energetically weaker C−H bonds of the carbon center.[52] This mode of reactivity has previously been observed for 9,10-dehydroanthracene and alkynyl porphyrins;[53-55] however, generally, enediyne reac-

(50) Bergman, R. G. *Acc. Chem. Res.* **1973**, *6*, 25−31.
(51) Rawat, D. S.; Zaleski, J. M. *J. Am. Chem. Soc.* **2001**, *123*, 9675−6976.
(52) Fossey, J.; Lefort, D.; Sorba, J. *Free Radical in Organic Chemistry*; Wiley: New York, 1995.

Scheme 4 Photothermal Cyclization of **3** in the Solid State

3
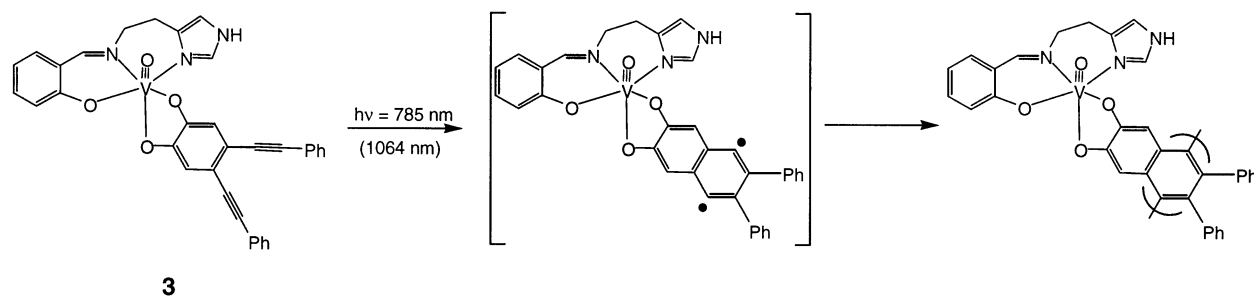
tivity of this nature is uncommon.[19,20,51] In addition to the unusual quenching mechanism, the reaction time and temperature necessary for significant (>50%) turnover are relatively high. Together these observations suggest the retrocyclization of the 1,4-phenyl diradical intermediate derived from **1** may significantly contribute to the overall reaction kinetics.[50] In the absence of a suitable donor, a radical−radical coupling or a radical insertion process becomes the dominant pathway, as evidenced by the formation of high molecular weight species from SEC analysis (Table 4). For **1b**, polymers of ∼11 000, with surprisingly narrow polydispersity (1.051), are clearly detected. Molecular weights of this magnitude are comparable to those which have been previously reported for the thermal polymerization of simple organic enediynes.[56]

The thermal reaction of **3** in the absence of H-atom donor also leads to the formation of high molecular weight species **3b** (Scheme 2). In contrast to the polymerization of **1**, reaction of the metal complex yields two broad features in the SE chromatogram with peak molecular weights of 17 160 and 5049 (Table 4). Polymers with molecular weights of ∼17 000 coarsely correspond to the M_w of ∼11 000 obtained for the oligomerization of **1** when the additional contribution of mass from the VO(SALIMH) portion of **3** is considered. The peak at 5049 may be associated with premature termination of polymer growth via intermolecular or intramolecular H-atom abstraction; however, detailed structural information of this nature is precluded by the large distribution of molecular weights (M_n) observed in these samples.

Photothermal Cyclization of 3 in the Solid State. Excitation of **3** in the solid state with 1064 nm from a Nd: YAG laser (10 Hz, 1 mJ/pulse), or a 785 nm diode laser (2 mW, 60 s) focused through a 50× objective, leads to photogeneration of a black material that is insoluble in many common solvents (Figure 5a,b; Scheme 4). Interestingly, the visual characteristics of the λ = 785 nm laser excitation on the bulk sample are similar to what is observed during the solid-state thermal reaction of **3**. Since photolyses of either **1** or **3** at 0 °C with λ ≥ 295 nm in solution (1000 W XeHg source) yields no reactivity after 24 h, we conclude that the observed photoreaction is not electronic in origin but rather
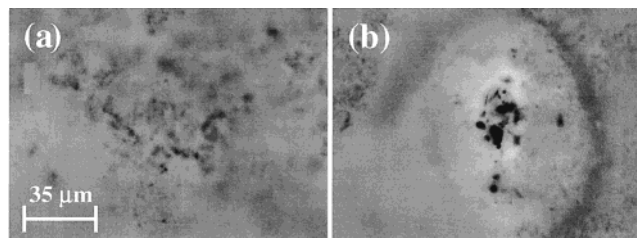
Figure 5. Color contrast images of the **3** in the solid state (a) before exposure to the 785 nm laser and (b) after exposure to 5 mW at 785 nm for 60 s.

must derive from a temperature-jumped thermal process via nonradiative excited-state decay (vide infra).

The temperature dependence of the Raman spectral profile obtained between 113 and 323 K at constant laser power (2 mW) illustrates the formation of the polymeric material (Figure 6). At low temperatures, the Raman spectrum is identical to the 80 K data shown in Figure 3b. However, as the temperature is raised between 203 and 283 K, a pronounced increase in the background fluorescence signal is observed. Distinct from the fluorescence background are very weak, emerging features at approximately 578, 1233, 1286, 1337, 1426, 1464, and 1590 cm^{-1} which cause the Raman spectrum (e.g. 243 K) to broaden in these regions, while vibrations at low frequency (100−500 cm^{-1}) remain relatively unchanged (Figure 6a,b). On the basis of the vibrational assignments in Table 3, these low-frequency features are most closely associated with the V−O stretches (ν_{48} and ν_{56}) involving the CatED ligand, as well as the CatED and SALIMH phenoxy C−O stretch and C=C ring stretches (ν_{126}, ν_{136}, ν_{141}, ν_{150}, ν_{155}, ν_{159}). The presence of similar vibrational features in the emerging spectrum of the photothermal product indicate that the V−O (CatED) and CatED ring units are intact in the product material.

Further increase in the temperature of the sample leads to enhanced fluorescence and the diffusion of most vibrational features into the background. The onset of fluorescence is not reversible as cooling to 80 K yields the same spectral profile as that shown at 323 K in Figure 6a. The irreversible increase in fluorescence is indicative of a photoinduced thermal reaction that generates a long wavelength emitting species. Indeed, heating of the sample to the temperature for the thermal Bergman cyclization reaction (246 °C) and subsequent analysis by Raman spectroscopy yields the same fluorescence background and broadened spectral profile as that obtained at higher temperatures (Figure 6a). The same increase in fluorescence is observed when the power

(53) Nath, M.; Zaleski, J. M. *J. Am Chem. Soc.*, manuscript in preparation.
(54) Aihara, H.; Jaquinod, L.; Nurco, D. J.; Smith, K. M. *Angew. Chem., Int. Ed.* **2001**, *40*, 3439−3441.
(55) Schottelius, M. J.; Chen, P. *J. Am. Chem. Soc.* **1996**, *118*, 4896−4903.
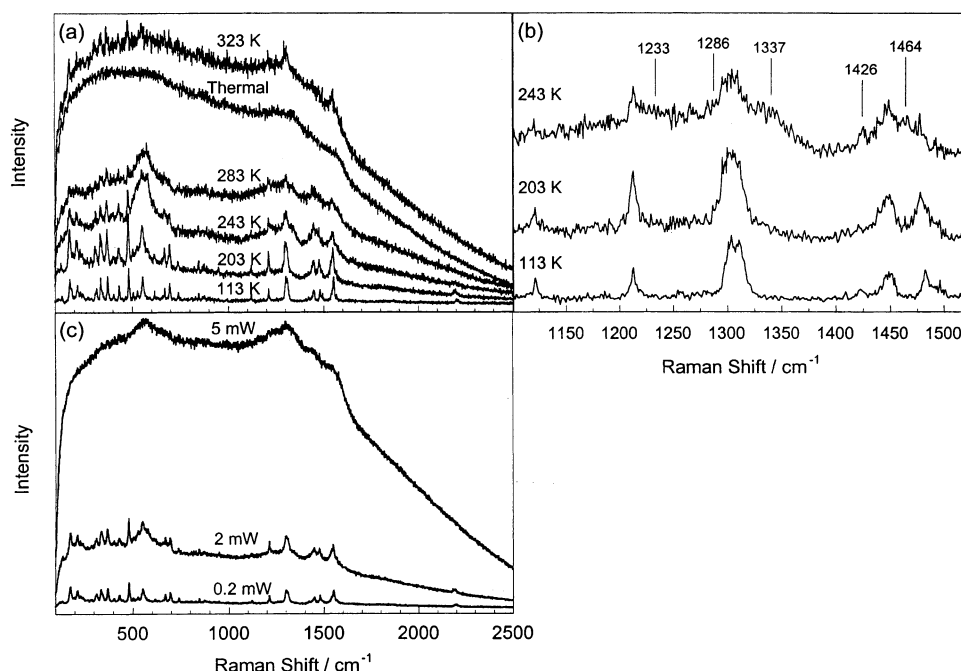(56) John, J. A.; Tour, J. M. *J. Am. Chem. Soc.* **1994**, *116*, 5011−5012.

Figure 6. (a) Temperature dependence (113−323 K) of the Raman spectrum of **3** in the solid state collected with 2 mW at $\lambda = 785$ nm for 60 s, along with the spectral profile (scaled intensity) of the thermal reaction product of **3** at 298 K. (b) Expansion of the 1050−1550 cm^{-1} region of the temperature-dependent spectra shown in a. (c) Power dependence (0.2, 2, and 5 mW) of the Raman spectrum of **3** obtained with $\lambda = 785$ nm at 298 K (60 s).

dependence (0.2−5 mW, 60 s) of the Raman spectrum is examined at room temperature (Figure 6c). At 0.2 mW, the Raman profile is very similar that obtained at 80 K and shown in Figure 3b. However, as the laser power is increased to 2 mW and finally 5 mW, a broad fluorescence background is once again produced, and broad vibrational features remain between ∼580−600, 1200−1350, and 1450−1600 cm^{-1}, indicative of V−O (CatED) and aromatic ring units in photothermally generated product.

Insight into the identity of black photothermal product can be obtained from a report documenting the generation of poly(*p*-phenylene) products upon thermolysis of simple enediynes in the solid state.[56] Vibrational characterizations of poly(*p*-phenylene) reveal strong luminescence and distinct features at 1216[57,58] (1222),[58] 1276 (1282), 1598 (1600) cm^{-1}, while metal-based electron donor/acceptor doped variants exhibit pronounced features at 1236, 1320, and 1600 cm^{-1}.[57,58] Similar vibrational analyses of alkyl substituted poly(*p*-phenylene) derivatives also show a strong interring C=C backbone feature at 1319 cm^{-1} and intraring signatures at 1554 and 1614 cm^{-1}.[59] Consequently, the increase in observed fluorescence and broadening of the CatED ring and V−O stretching regions due to the presence of new vibrational features (578, 1233, 1286, 1337, 1426, 1464, and 1590 cm^{-1}) suggest the formation of oligomeric units of metallo−poly(*p*-phenylene) products generated by near-IR,

photothermal Bergman cyclization of molecular enediyne units. Although radical−radical coupling products such as these are expected, they are likely not exclusive, as radical insertion products involving unsaturated carbon linkages may also be formed.[60]

The generation of polymeric structures from thermolysis of **3** (vide supra) supports the oligomerization reaction proposed from the in situ optical/vibrational characterization of the photothermal cyclization reaction upon $\lambda = 785$ nm excitation. Indeed, the formation of extended molecular structures via a photothermal mechanism is confirmed by SEC analyses of solid-state samples exposed to $\lambda = 785$ nm. Photothermal excitation of **3** leads to the formation of high molecular weight species **3c** (Scheme 2, Table 4) possessing a $M_w = 5600$ and an average molecular weight of $M_n = 4170$. The polydispersities of **1b** and **3c** are notably low, indicating that, in addition to the obvious radical polymerization scheme, alternative radical polymerization mechanisms may be possible.[56,60,61] The M_w value corresponds to an average of 9−10 monomeric units of **3**, assuming nominal degradation of the starting molecular structure. Overall **3c** is of lower average molecular weight than **3a**. This is easily rationalized by considering the difference in polymerization conditions; **3a** was generated through uniform heating of the entire sample volume, while **3c** is obtained upon successive exposures of small fractions of the sample that incrementally react in local regions. This can lead to termination steps and decreased polydispersity. Regardless of the average molecular weight or distribution of molecular weights, these results demonstrate that a photothermal pathway via nonradiative

(57) Krichene, S.; Buisson, J. P.; Lefrant, S.; Froyer, G.; Maurice, F.; Goblot, J. Y.; Pelous, Y.; Fabre, C. *Mol. Cryst. Liq. Cryst.* **1985**, *118*, 301.
(58) Krichene, S.; Lefrant, S.; Froyer, G.; Maurice, F.; Pelous, Y. *J. Phys. Colloq.* **1983**, *44*, 733.
(59) Godon, C.; Buisson, J. P.; Lefrant, S.; Sturm, J.; Klemenc, M.; Graupner, W.; Leising, G.; Mayer, M.; Schluter, A. D.; Scherf, U. *Synth. Met.* **1997**, *84*, 673−674.

(60) Grissom, J. W.; Calkins, T. L. *J. Org. Chem.* **1993**, *58*, 5422−5427.
(61) Webster, O. W. *Science* **1991**, *251*, 887−893.

excited-state decay can be a viable approach not only to initiating Bergman cyclization but also to the generation of extended molecular structures.

Conclusions

Herein a unique approach for photoinitiating Bergman cyclization has been described. Rather than photochemically promoting cyclization via electronic excitation using ultraviolet photons, we have introduced a strongly absorbing oxygen-to-V(V) LMCT transition at 1028 nm, which when pumped with near-IR photons ($\lambda = 785$ nm), leads to polymeric material with spectral characteristics consistent with the formation of metallo−poly(*p*-phenylene) products derived from Bergman cyclization. This conceptual study reveals two new potential opportunities: first designing photothermally activated agents for photodynamic therapy applications that can be triggered using tissue transparent near-IR photons and, second, the photothermally induced polymerization of unsaturated hydrocarbons. The engineering of molecular designs that preserve the electronic structure

and desirable optical properties of the compound while exhibiting more facile thermal reactivities for low laser power applications is very plausible on the basis of existing metalloenediyne structures and is currently underway.

Supporting Information Available: Crystallographic data including complete tables of bond distances and angles, final fractional coordinates, and thermal parameters and figures of the thermal ellipsoid of **3** and various IR and Raman spectra (PDF). This material is available free of charge via the Internet at http://pubs.acs.org.

IC0207045